Available online at www.sciencedirect.com

ScienceDirect

Procedia CIRP 18 (2014) 120 – 125

www.elsevier.com/locate/procedia

International Conference on Manufacture of Lightweight Components – ManuLight2014

A Comparison of FSW, BHLW and TIG Joints for Al-Si-Mg alloy (EN AW-6082 T6)

V. Walter[1]*, K. A. Weidenmann[1], V. Schulze[1]

[1] Institute for Applied Materials IAM-WK, Karlsruhe Institute of Technology (KIT), Germany

* Corresponding author. Tel.: +49 (0) 721 608 46595; fax: +49 (0) 721 608 48044; *E-mail address*: Volker.Walter@kit.edu

Abstract

For joining lightweight frame structures, two welding methods are within the focus of the Transregional Collaborative Research Centre SFB/TR 10. The first one is the friction stir welding (FSW) and the second one is the bifocal hybrid laser welding (BHLW). To compare the properties of joints manufactured using these techniques with tungsten inert-gas welding (TIG), representing a conventional joining method, a benchmark was performed. This benchmark includes a comparison of the microstructure, the pore distribution, the microhardness and the mechanical behavior at quasi-static and high-speed tensile loading. The results reveal that the BHLW and the FSW processes outperform the TIG process regarding the mechanical properties of the joints produced.

Peer-review under responsibility of the International Scientific Committee of the "International Conference on Manufacture of Lightweight Components – ManuLight 2014"

Keywords: Friction stir welding; Bifocal hybrid laser welding; Tungsten inert-gas welding; AW-6082, T6.

1. Introduction

Currently the weight reduction of motor vehicle body components is mostly reached by using lightweight materials like aluminum and thin-walled structures. Therefore, joining technologies are demanded which can produce joints of high strength for the manufacturing of lightweight frame structures. Inside the Collaborative Research Center SFB/TR10 "Integration of forming, cutting and joining for the flexible production of light-weight space frame structures", one focus lies on two joining technologies to achieve this aim. The first one is the friction stir welding (FSW), a solid state joining technique. Advantages here are low residual stress and distortion, a reduced amount of defects like cracks and pores and the ability to join hardy weldable materials [1]. The second technology is the bifocal hybrid laser welding (BHLW). The combination of a Nd:YAG-laser and a high power diode laser allows a high welding speed [2] with a low pore density and a small heat impact.

In the present work, a comparison between these two relatively novel techniques with a long established one, the tungsten inert-gas welding (TIG), will show their advantages. The used material, EN AW-6082 T6, makes high claims to these techniques due to the problems of pore formation and hot cracks [3]. Another problem is the loss of hardness and strength caused by the micro-structural instability in the heat affected zone (HAZ) [4].

2. Material and experimental procedure

2.1. Material and welding processes

The base material were rolled, 2 mm thick sheets of EN AW-6082 (AlSiMg1) in the state T6 which means, they were solution-annealed, water quenched and artificially aged. For this work, these sheets were butt welded with different methods. The chemical composition is shown in Tab. 1.

The joining processes FSW [5] and BHLW [6] were performed at the Institute for Machine Tools and Industrial Management of Technical University of Munich (Germany). The parameters used for FSW were a welding speed of 400 mm/min and a pin rotation speed of 1500 rpm. The pin features an average diameter of 2 mm, the shoulder diameter was 13 mm at a pitch of 2°.

Peer-review under responsibility of the International Scientific Committee of the "International Conference on Manufacture of Lightweight Components – ManuLight 2014"
doi:10.1016/j.procir.2014.06.118

Table 1. Chemical composition of EN AW-6082 [8] and EN AL-4047 A [9]

	Si	Fe	Cu	Mn	Mg	Cr	Ni	Zn	others	Ti	Rest
unit	%	%	%	%	%	%	%	%	%	%	%
EN AW-6082	0.7-1,3	0.5	0.1	0.4-1.0	0.6-1.2	0.25	-	0.2	0.15	0.1	AL
EN AL-4047A	11.0-13.0	0.6	0.3	0.15	0.1	-	-	0.2	0.15	0.15	AL

To reduce porosity content in the BHLW weld seam, the edges of the sheets were cleaned with a scraper and polishing fleece before joining [7].
The Nd:YAG-laser power was set to 3 kW, the HPDL power to 4.1 kW. The used welding speed (v_w) was 3.75 m/min and the filler wire of EN AL-4047A (AlSi12) with a diameter of 1 mm had a speed (v_{fw}) of 4.13 mm/min. The alloy composite of the filler wire is given in Tab. 1. The TIG welds with the same filler were performed by a certified welding operator.

2.2. X-ray micro-computed tomography

In order to get information about the pore density and their distribution as well as the presence of hot cracks, 3D CT-scans were performed. An Yxlon-CT precision computed tomograph with an open micro-focus X-ray transmission tube with tungsten target and a flat panel detector with 2048x2048 pixels from Perkin Elmer® was used for imaging. Each scan consists of 2010 projections during a 360° rotation along the vertical axis (i.e. one projection every 0.18°) with an integration time of 700 ms. The accelerating voltage was set to 140 kV and the accelerating current to 0.06 mA. With Avizo® Fire from VSG and ImageJ, a segmentation of pores and solid material was possible. This allows the determination of the volume fraction of pores in the fusion zone.

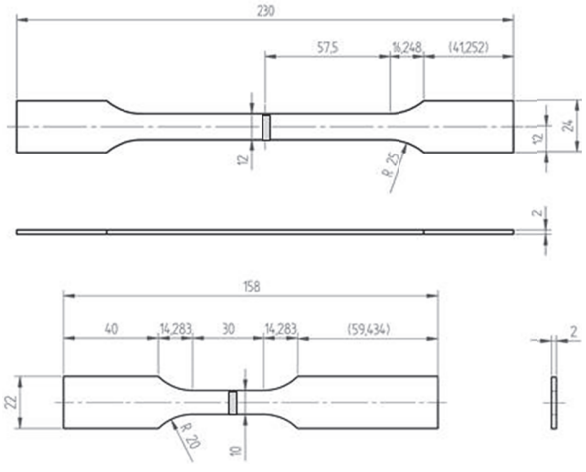

Fig. 1. Sample geometries of the quasi-static (top) and the high-speed (bottom) tensile tests (unit: mm)

2.3. Microstructural studies and hardness measurement

A sample of each welding process was extracted in order to determine the weld seam geometry as well as the microstructure inside the weld seam and in the HAZ. These samples were anodically etched with Barker`s reagent [10] and observed by an light optical microscope (LOM) from Carl Zeiss using polarized light.

Information about changes of the heat treatment through the welding processes was obtained by determination of micro hardness profiles perpendicular to the welding direction with a Qness Q10A+. Therefore, Vickers HV 0.2 indentations with a distance of 0.5 mm were set until the origin hardness of the base material (116-118 HV 0.2) was reached.

2.4. Mechanical tests

In order to determine the quasi-static tensile properties of the welds, specimens were taken from every process with geometry according to DIN EN ISO 4136 [11] (Fig. 1. top). In each case the weld seam was located in the middle of the sample`s measuring section and perpendicular to the test direction. These tests were carried out in a 200 kN Zwick Roell machine with a strain rate ($\dot{\varepsilon}$) of 0.005 1/s.

Furthermore high-speed tensile tests with a strain rate ($\dot{\varepsilon}$) of 200 1/s were carried out in an Amsler HTM 5020 Zwick Roell machine. The weld seam is located in the middle of the sample`s measuring section which is analogue to the quasi-static tensile tests. Fig. 1. bottom gives the geometry of these samples.

3. Results

3.1. Pore distribution and cracks

As expected, in the whole volume of the FSW weld seam, no pores or cracks can be found (Fig. 2. top).

The highest pore density with 0.83 % of the fusion zone volume can be found in the BHLW weld seam which contains two types of pores. There are a few larger ones close to the upper surface with a volume up to 0.00652 mm^3 and some smaller ones, mostly near the lower surface (Fig. 2. middle). These pores might result from entrapped hydrogen or shielding gas. The median pore volume was determined to $4.14*10^{-7}$ mm^3. The

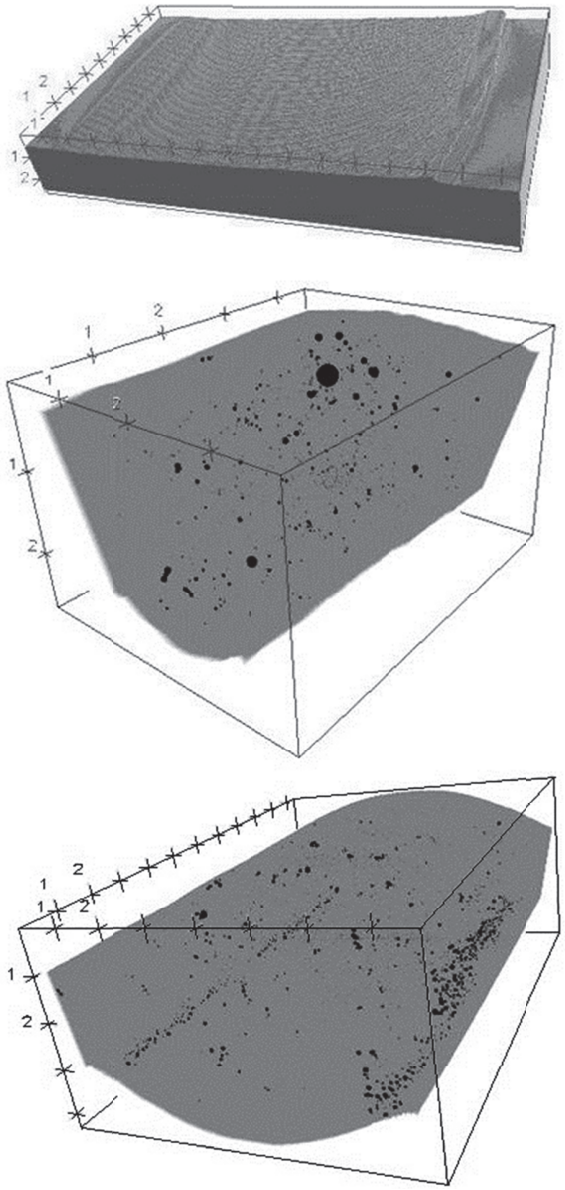

Fig. 2. Pore distribution in the FSW (top), BHLW (middle) and TIG (bottom) weld seam (unit: mm)

absence of cracks in the complete scanned sample shows, that the amount of filler wire is sufficient.

There are also two types of pores in the TIG fusion zone with a volume fraction of 0.52 %, a seam of small ones near the lower surface close to the non-melted material and some large pores in the middle of the weld seam (Fig. 2. bottom). The largest pore has a volume of $7.96*10^{-4}$ mm^3 and the median volume of all pores is $3.65*10^{-7}$ mm^3. Like in the BHLW joined sample, no cracks could be identified.

3.2. Microstructural studies and hardness measurement

The microstructure of the FSW joined sample can be separated into three zones, in the middle a nugged zone followed by a thermo-mechanically affected zone (TMAZ) and the HAZ. Due to high plastic deformation and high temperature during the welding process inside the nugged zone, recrystallization occurred, resulting in a very fine grained microstructure (Fig. 3. a middle) [1]. Inside the TMAZ, deformed grains from the parent material can be found (Fig. 3. a left). In the HAZ no microstructural changes are with a LOM. The grain structure and the grain size are unchanged compared with the parent material (Fig. 3. a right).

The shape of the fusion zone from the BHLW process is defined by the power distribution of the combined lasers [12]. In the center of the zone, a typical microstructure of a fusion welded sample with big grains and very fine dendritic structures can be seen (Fig. 3. b middle). The top surface displays a smooth transit between the fusion zone and the base material. At the bottom

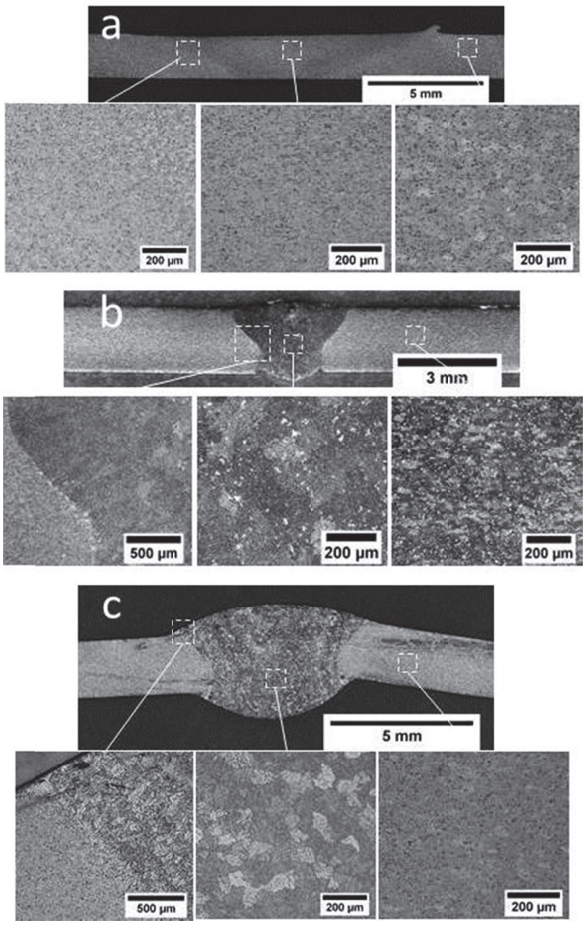

Fig. 3. Microstructure of the FSW (a), BHLW (b) and TIG weld seam (c)

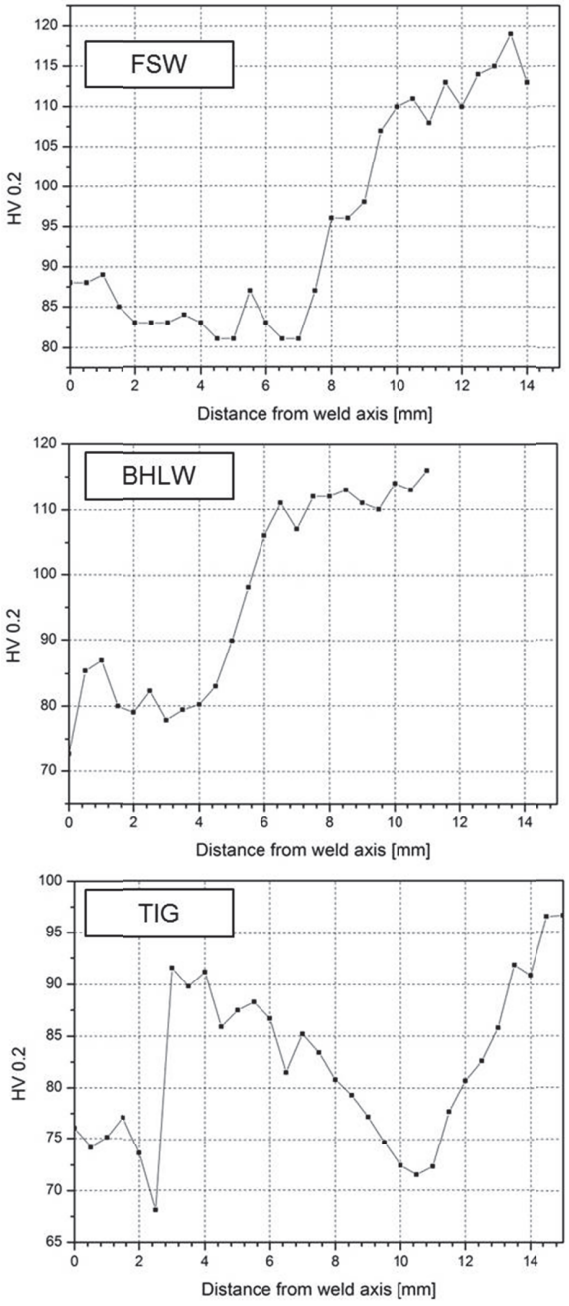

Fig. 4. Hardness profile of the FSW (top), BHLW (middle) and the TIG sample (bottom)

surface a notch can be found on both sides. Inside the material, this intersection is very sharp and no influence to the grains nearby can be found (Fig. 3. b left). In the HAZ no microstructural change compared to the parent material can be determined (Fig.3. b right).

The TIG joined sample shows also a microstructure with large grains and dendritic structures inside the weld seam (Fig. 3. c middle). These structures are not as fine as in the BHLW weld seam. Fig. 3. c –left shows the intersection between the parent material and the fusion zone. The microstructure in the HAZ (Fig. 3. c right) does not feature any changes from the welding process.

The hardness profile of the FSW joined sample shows a significant softening in the welding zone (Fig. 4. top). A minimum of hardness can be found inside the HAZ. This softening can be explained by the reduction of needle-shaped precipitations caused by the process temperature [13]. Outside the HAZ, the origin hardness of the base material is reached again.

As shown in Fig. 4. middle, the center of the weld seam represents the hardness minimum at the BHLW sample. This minimum is followed by a plateau until the border of the HAZ is reached at a distance from 4.5 mm to the weld axis. In this region, overageing leads to a reduced hardness. The original hardness of the parent material can be measured outside the HAZ.

Fig. 4. bottom shows the hardness profile of the TIG joined sample up to a distance from the weld axis of 15 mm. Inside the HAZ the hardness is reduced compared to the base material. Inside the HAZ, hardness is highest between the melted zone and 9.5 mm from the weld axis. Here, the heat from the process was high enough for a solutionizing and the cooling rate from self-quenching was fast enough to form fine precipitates [14]. The big grains in the melted zone, up to 2.5 mm from the weld axis, are leading to a lower hardness. Between 9.5 mm and 11 mm from the weld axis, due to overageing, the hardness declines to a value lower than in the melted zone. Outside this low hardness zone, the hardness is continuously rising and the origin hardness of the base material is reached after 24 mm.

3.3. Tensile Tests

Representative stress-strain plots of the quasi-static

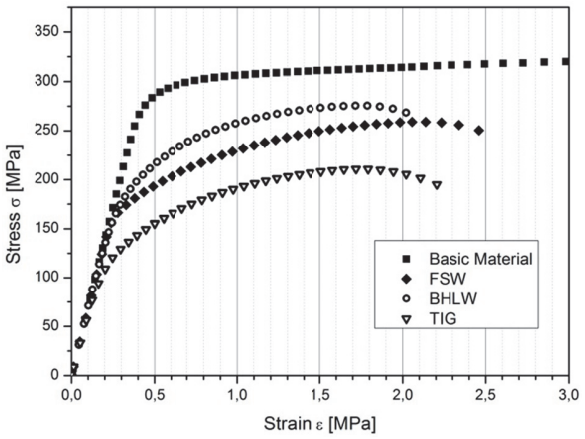

Fig. 5. Quasi-static stress-strain curve

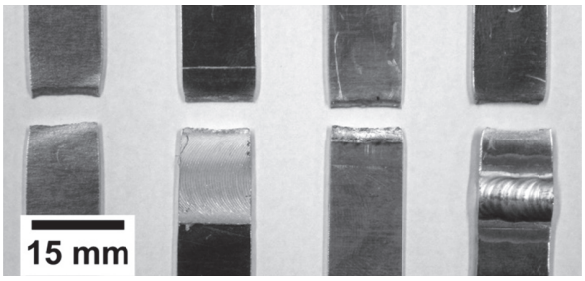

Fig. 6. Fractured quasi-static tensile samples, from left: Base Material, FSW, BHLW, TIG

tensile tests are presented in Fig. 5. An explicit order can be seen, both for the yield strength and the ultimate tensile strength. Despite the fact that joining by FSW produces a pore- and crack-free weld seam with a small grain size, the samples joined by BHLW have a higher strength. As expected, the TIG joined samples show the lowest strength. As seen in Fig. 6., the fracture location can be correlated to the decline of hardness in the HAZ. This effect is already described in [4]. Necking occurred on both sides of the weld seam. Because of the notch effect, the FSW joined samples fracture at the intersection between the weld seam and the base material at the retreating side similar to [15]. Also the majority of the BHLS joined samples are failing at the intersection, but some samples are breaking in the HAZ. The failure point does not have a significant influence to the reached strength.

If the strain rate ($\dot{\varepsilon}$) is increased to 200 1/s, the ultimate tensile strength rises in all samples compared to the quasi-static test (Fig. 7). This is due to viscous-drag and already observed for non-welded EN AW-6082 T6 [16]. In contrary to the quasi-static load, FSW joined samples have a higher strength than the BHLW joined ones. This can be an effect of the modified composition in the fusion zone by the filler wire or the modified microstructure by the fusion. The point of failure is similar to the quasi-static load.

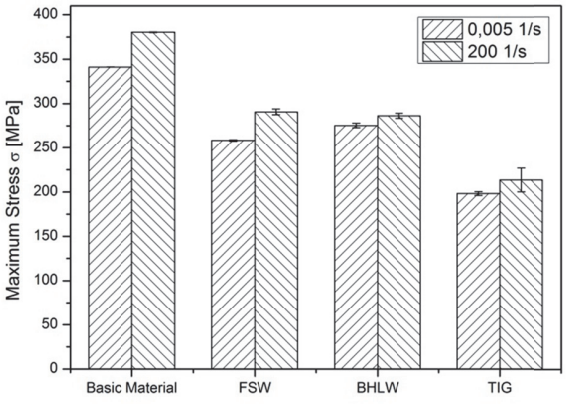

Fig. 7. Strain rate influence on the ultimate tensile strength

4. Summary

The present work shows, that the FSW and the BHLW process have advantages compared to the TIG process. With FSW, joints free of pores and cracks can be produced with a minimum of heat impact. Both fusion welding processes do not achieve a weld seam without pores, but cracks can be avoided.

The BHLW produces the joints with the highest quasi-static tensile strength followed by the FSW and the TIG process. If a high strain rate is used, the BHLW and the FSW process change their ranking order. The heat impact and the associated overageing and hardness lost are reduced compared to the TIG process.

A further reduction of pores in the BHLW weld seam would not lead to a significant higher quasi-static tensile strength, because the samples that failed in the HAZ do not lead to better results. Hence, just a change of the location of the fracture from the intersection to the HAZ would be expected.

Acknowledgements

The work is based on the investigations of the subproject A9- “Relation between Structure and Properties of Joints” - of the Transregional Collaborative Research Center/Transregio 10, which is kindly supported by the German Research Foundation (DFG). The authors would also like to thank the Institute for Machine Tools and Industrial Management of the Technische Universität München for welding the FSW and BHLW samples.

References

[1] Mishra, R.S.; Ma, Z.Y.: Friction stir welding and processing. Materials Science and Engineering R 50 (2005) pp. 1-78

[2] Schulze, V.; Löhe, D.; Barreiro, P., Einfluss kombinierter Nd:YAK- und Hochleistungsdioden-Laserstrahlschweißprozesse auf die mechanischen Eigenschaften von Al6060 bei quasistatischer Beanspruchung. Aluminium, International Journal for Industry, Research and Application, 80 (2004) 12, pp. 1392-1396

[3] Miyazaki, M.; Nishio, K.; Katoh, M.; Muake, S.; Kerr, W., Quantitative Investigation of Heat-Affected Zone Cracking in Aluminum Alloy 6061. Welding Research Supplement, 69 (1990) 9, pp. 362-371

[4] Malin, V., Study of Metallurgical Phenomena in the HAZ of 6061-T6 Aluminum Welded joints. Welding Research Supplement, 74 (1995) 9, pp. 305-318

[5] Ruhstorfer, M.; Zaeh, M. F.: Friction Stir Welding of Steel Reinforced Aluminium Extrusions. 7th International Friction Stir Welding Symposium, Awaji Island, Japan 2008

[6] Zaeh, M. F.; Trautmann, A., Vergleich des hybriden, bivokalen Laserschutzgasschweißens mit Laser-MIG-Hybridverfahren. Aluminium 80 (2004) 12. pp. 1387-91

[7] Haboudou, A.; Peyre, P.; Vannes, A.B.; Peix, G., Reduction of porosity content generated during Nd:YAG laser welding of A356 and AA5083 aluminium alloys. Materials Science and Engineering, A363 (2003). pp. 42-50

[8] CEN European Committee for Standardization, Aluminium and aluminium alloys - Chemical composition and form of wrought products - Part 3: Chemical composition and form of products, EN 573-3, 2009-04-00.
[9] DIN EN ISO 18273. Schweißzusätze - Massivdrähte und -stäbe zum Schmelzschweißen von Aluminium und Aluminiumlegierungen – Einteilungen. Deutsche Fassung EN ISO 18273: 2004
[10] Petzow, G., Metallographisches Keramographisches Plastographisches Ätzen. In: Materialkundlich-technische Reihe 1, Gebrüder Bornträger, Berlin, 1994
[11] DIN EN ISO 4136. Zerstörende Prüfung von Schweißverbindungen an metallischen Werkstoffen – Querzugversuch. Deutsche Fassung EN ISO 4136: 2011
[12] Huber, S.; Merzkirch, M.; Zaeh, M.F.; Schulze, V., Applications of High-Power Diode Lasers for Aluminum Welding. SPIE Proceedings, High-Power Diode Laser Technology and Applications VII, Volume 7198 (2009)
[13] Sato, Y.S.; Kokawa, H.; Enmoto, M.; Jogan, S., Microstructural Evolution of 6063 Aluminum during Friction-Stir Welding. Metallurgical and Materials Transactions, Volume 30A, (1999) pp. 2429-2437
[14] Kramer, L.S.; Pickens, J.R., Microstructure and Properties of a Welded Al-Cu-Li Alloy. Welding Journal Volume 71(4) (1992), pp. 115-121
[15] Sato, Y.S.; Kokawa, H., Distribution of tensile property and microstructure in friction stir weld of 6063 aluminum. Metallurgical and Materials Transactions, Volume 32A, (2001) pp. 3023-3031
[16] Moćko, W.; Rodríguez-Martínez, J.A.; Kowalewski, Z.L.; Rusinek, A., Compressive Viscoplastic Response of 6082-T6 and 7075-T6 Aluminium Alloys Under Wide Range of Strain Rate at Room Temperature: Experiments and Modeling. Strain, An International Journal for Experimental Mechanics, 48 (2012) 6, pp. 498-509